A Kinematically Redundant Hybrid Robot for Low-Impedance Physical Human-Robot Interaction

Kefei Wen, Tan Sy Nguyen, David Harton, Thierry Laliberté and Clément Gosselin

***Abstract*— In this paper, we propose a $(6 + 3)$-degree-of-freedom kinematically redundant hybrid robot for low-impedance physical human-robot interaction. The architecture of the robot allows all actuators to be placed very close to the base, thus reducing the inertia of the moving parts. Moreover, such an arrangement makes it possible to use larger direct-drive motors. The direct-drive motors ensure the backdrivability of the robot, which makes the physical human-robot interaction effortless, i.e., the mechanical interaction between the robot and the human user has a low impedance and a high bandwidth. Therefore, the robot can be controlled using an impedance control approach and no force/torque sensor is required. The low mechanical impedance of the interaction yields a very intuitive and reactive behaviour since no force control loop is involved. Moreover, the design of the hybrid parallel robot exploits redundancy to avoid Type II singularities, leading to a very large orientational workspace.**

I. Introduction

In most serial robots, small motors with high gear reductions are used, especially for the distal joints, in order to reduce the inertia of the moving parts and improve the output torques. As a consequence, such a robot is generally not backdrivable and hence a force/torque sensor is necessary in applications that involve physical human-robot interaction (pHRI). The use of a parallel robot has the potential to overcome these drawbacks. In most cases, all actuators of a parallel robot are evenly distributed in its legs, which greatly increases the load-bearing capacity of the robot and low gear reduction motors can be used if the robot is actuated by revolute joints. Also, the joints which are close to the base can be chosen as the actuated ones in order to reduce the inertia of the moving parts of the robot as much as possible. Implementing pHRI using parallel robots was investigated, for instance, in [1]–[3]. However, applications of most non-redundant parallel mechanisms are still limited mainly due to the inevitable type II singularities [4], which considerably reduce the effective workspace, especially for rotations.

An effective way to alleviate type II singularities and to enlarge the useful workspace of a parallel robot is by introducing kinematic redundancy. In this paper, we propose a 3-[R(RR-RRR)SR] $(6 + 3)$-degree-of-freedom (DoF) kinematically redundant hybrid robot (KRHR) for pHRI applications. Here, R denotes an actuated revolute joint, R a passive revolute joint and S a passive spherical joint. As shown in Fig. 1, in each leg, the axis of the first R joint is parallel to the base plane while the axis of the distal R joint attached to the platform is orthogonal to the platform plane, the axes of the rest of the revolute joints are parallel to each other and orthogonal to that of the first R joint. This KRHR uses a direct drive transmission in order to produce backdrivability. The robot was first introduced in [5], where is was shown that the proposed architecture has very simple singularity conditions and that all singularities can either be avoided or eliminated. It was also shown that an analytical inverse kinematic solution can be derived for the proposed KRHR, which makes it straightforward to operate a gripper on the moving platform from the base actuators by utilizing the redundancies [5].

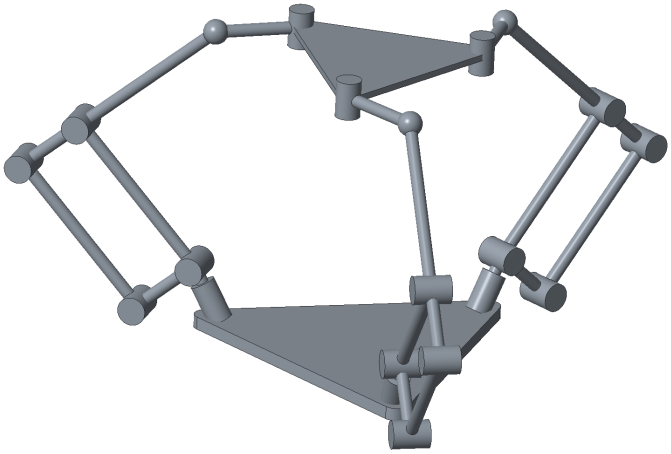

Fig. 1. Kinematic architecture of the proposed hybrid robot.

In the next section, the velocity equations and the singularity analysis of the proposed robot are recalled. Methods for the development of the forward and inverse kinematic problems are provided in Section III. Translational and orientational workspaces are evaluated in Section IV. The control of the robot in a pHRI mode is then presented in Section V. Finally, conclusions are drawn in Section VI. Some design and control issues are then addressed in Sections V and VI, respectively.

II. Velocity Equations and Singularity Analysis

A. Velocity Equations

The derivation of the velocity equations of this architecture was presented in [5] and is briefly recalled here. For each leg, a constraint equation on the length of the redundant link

*The financial support of the Natural Sciences and Engineering Research Council of Canada (NSERC) and of the Canada Research Chair program is gratefully acknowledged.

The authors are with the Robotics Laboratory, Department of Mechanical Engineering, Université Laval, Québec, QC, Canada, kefei.wen.1@ulaval.ca; david.harton.1@ulaval.ca; thierry@gmc.ulaval.ca; tan-sy.nguyen.1@ulaval.ca; gosselin@gmc.ulaval.ca

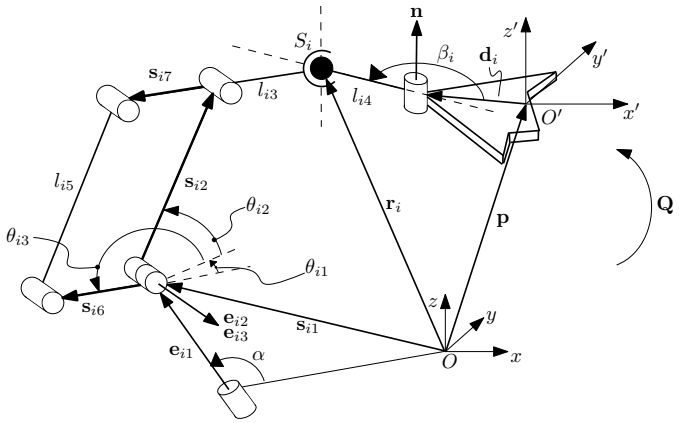

Fig. 2. Kinematic description of one leg of the robot.

(l_{i4}) can be written as

$$(\mathbf{p} + \mathbf{Q}\mathbf{d}_i - \mathbf{r}_i)^T (\mathbf{p} + \mathbf{Q}\mathbf{d}_i - \mathbf{r}_i) = l_{i4}^2 \tag{1}$$

where $\mathbf{r}_i$ is the position vector of the centre of the ith spherical joint, $\mathbf{p}$ and $\mathbf{Q}$ are the position and orientation of the platform and $\mathbf{d}_i$ is the vector connecting the origin of the platform frame to the revolute joint attached to the platform, as indicated in Fig. 2. Also, the fourth link must be orthogonal to the axis of the R joint attached to the platform, which yields

$$\mathbf{n}^T (\mathbf{p} + \mathbf{Q}\mathbf{d}_i - \mathbf{r}_i) = 0 \tag{2}$$

where the unit vector $\mathbf{n}$ is

$$\mathbf{n} = \mathbf{Q}[\boldsymbol{z}']_{O'} \tag{3}$$

where $[\boldsymbol{z}']_{O'} = [0\ 0\ 1]^T$ represents the $\boldsymbol{z}'$ axis expressed in the platform frame and is perpendicular to the platform plane.

The Cartesian velocities of the platform and actuated joint velocities can be respectively expressed as

$$\mathbf{t} = [\dot{\mathbf{p}}^T\ \boldsymbol{\omega}^T]^T \tag{4}$$

$$\dot{\boldsymbol{\theta}} = [\dot{\boldsymbol{\theta}}_1^T\ \dot{\boldsymbol{\theta}}_2^T\ \dot{\boldsymbol{\theta}}_3^T]^T \tag{5}$$

with $\dot{\boldsymbol{\theta}}_i = [\dot{\theta}_{i1}\ \dot{\theta}_{i2}\ \dot{\theta}_{i3}]^T$. The dimension of vector $\mathbf{t}$ is 6×1 while it is 9×1 for vector $\dot{\boldsymbol{\theta}}$. The Jacobian matrices can be obtained by differentiating the constraint equations, which yields

$$\mathbf{J} = \begin{bmatrix} \mathbf{a}_{14}^T & [(\mathbf{Q}\mathbf{d}_1) \times \mathbf{a}_{14}]^T \\ \mathbf{n}^T & (\mathbf{c}_1 \times \mathbf{n})^T \\ \mathbf{a}_{24}^T & [(\mathbf{Q}\mathbf{d}_2) \times \mathbf{a}_{24}]^T \\ \mathbf{n}^T & (\mathbf{c}_2 \times \mathbf{n})^T \\ \mathbf{a}_{34}^T & [(\mathbf{Q}\mathbf{d}_3) \times \mathbf{a}_{34}]^T \\ \mathbf{n}^T & (\mathbf{c}_3 \times \mathbf{n})^T \end{bmatrix} \tag{6}$$

which is of dimension 6×6 and in which

$$\mathbf{a}_{i4} = \mathbf{p} + \mathbf{Q}\mathbf{d}_i - \mathbf{r}_i, \quad i = 1, 2, 3 \tag{7}$$

$$\mathbf{c}_i = \mathbf{Q}\mathbf{d}_i - \mathbf{a}_{i4} \tag{8}$$

and

$$\mathbf{K} = \begin{bmatrix} \mathbf{a}_{14}^T\mathbf{M}_1 & \mathbf{0} & \mathbf{0} \\ \mathbf{n}^T\mathbf{M}_1 & \mathbf{0} & \mathbf{0} \\ \mathbf{0} & \mathbf{a}_{24}^T\mathbf{M}_2 & \mathbf{0} \\ \mathbf{0} & \mathbf{n}^T\mathbf{M}_2 & \mathbf{0} \\ \mathbf{0} & \mathbf{0} & \mathbf{a}_{34}^T\mathbf{M}_3 \\ \mathbf{0} & \mathbf{0} & \mathbf{n}^T\mathbf{M}_3 \end{bmatrix} \tag{9}$$

which is of dimension 6×9 while $\mathbf{0}$ is the 1×3 zero matrix. The matrix $\mathbf{M}_i, i = 1, 2, 3$ is the Jacobian of the ith RR-RRR linkage and is obtained as

$$\mathbf{M}_i = \mathbf{J}_i^{-1}\mathbf{W}_i, \quad i = 1, 2, 3 \tag{10}$$

where

$$\mathbf{J}_i = \begin{bmatrix} \mathbf{e}_{i2}^T \\ \mathbf{v}_i^T \\ -\frac{l_{i7}}{l_{i3}}\mathbf{u}_i^T \end{bmatrix} \tag{11}$$

and

$$\mathbf{W}_i = \begin{bmatrix} w_{i11} & 0 & 0 \\ 0 & \mathbf{v}_i^T(\mathbf{e}_{i2} \times \mathbf{s}_{i2}) & 0 \\ 0 & w_{i32} & \mathbf{u}_i^T(\mathbf{e}_{i3} \times \mathbf{s}_{i6}) \end{bmatrix} \tag{12}$$

with

$$w_{i11} = (\mathbf{r}_i - \mathbf{s}_{i1})^T(\mathbf{e}_{i2} \times \mathbf{e}_{i1}) \tag{13}$$

$$w_{i32} = (1 + \frac{l_{i7}}{l_{i3}})\mathbf{u}_i^T(\mathbf{s}_{i2} \times \mathbf{e}_{i2}) \tag{14}$$

$$\mathbf{v}_i = \mathbf{r}_i - \mathbf{s}_{i1} - \mathbf{s}_{i2} \tag{15}$$

$$\mathbf{u}_i = \mathbf{s}_{i2} + \mathbf{s}_{i7} - \mathbf{s}_{i6} \tag{16}$$

and where the unit vector $\mathbf{e}_{ij}, j = 1, 2, 3$ is the direction cosines of the corresponding actuated joint.

B. Singularity Analysis

In the ith leg, type I singularities occur whenever matrix $\mathbf{W}_i$ is singular, which happens if one of the following conditions is satisfied:

1) the centre of the spherical joint lies on the axis of the first revolute joint, in which case $w_{i11} = 0$;
2) $\mathbf{v}_i$ is orthogonal to $(\mathbf{e}_{i2} \times \mathbf{s}_{i2})$;
3) $\mathbf{u}_i$ is orthogonal to $(\mathbf{e}_{i3} \times \mathbf{s}_{i6})$.

Since in matrix $\mathbf{J}_i$, vector $\mathbf{e}_{i2}$ is always perpendicular to both vectors $\mathbf{v}_i$ and $\mathbf{u}_i$, a type II singularity in this leg occurs only when these two vectors are aligned. These configurations are easily avoided in practice. In summary, the possible singularities of the legs are easily handled.

A type II singularity of the moving platform occurs whenever the Jacobian $\mathbf{J}$ defined in (6) becomes singular. The singularity conditions are quite simple and can be classified as:

1) the three coplanar Plücker line $[\mathbf{a}_{i4}^T\ [(\mathbf{Q}\mathbf{d}_i) \times \mathbf{a}_{i4}]^T], i = 1, 2, 3$ intersect at a common point or are parallel to each other;
2) when the three parallel Plücker lines $[\mathbf{n}^T\ [(\mathbf{c}_i) \times \mathbf{n}]^T], i = 1, 2, 3$ become coplanar.

The former case can be avoided by reorienting one of the three redundant links while the latter case is simply

eliminated in practical designs by making the redundant links relatively short compared to the size of the moving platform to ensure that no straight line can simultaneously intersect the centres of all three spherical joints.

III. Forward and Inverse Kinematics

A. Forward Kinematics

The three legs of the hybrid parallel robot each contain 3 actuators. From the kinematics of the legs, it is straightforward to compute the position of the spherical joints (vectors $\mathbf{r}_i$) for given values of the actuated joint coordinates. Indeed, each leg consists in an actuated revolute joint in series with a planar 5-bar 2-dof parallel mechanism, whose forward kinematics is straightforward. In order to complete the forward kinematics of the robot, the position and orientation of the platform are then computed from the position of the spherical joints using a numerical procedure.

First, matrix $\mathbf{Q}$, which represents the orientation of the platform, is defined as $\mathbf{Q} = [\mathbf{q}_x \ \mathbf{q}_y \ \mathbf{q}_z]$, where the last column, noted $\mathbf{q}_z$, is the vector $\mathbf{n}$ shown in (3) and can be obtained from

$$\mathbf{q}_z = \frac{\mathbf{r}_{12} \times \mathbf{r}_{13}}{\| \mathbf{r}_{12} \times \mathbf{r}_{13} \|} \tag{17}$$

where $\| \cdot \|$ denotes the Euclidean norm of its vector argument and $\mathbf{r}_{1j} = \mathbf{r}_j - \mathbf{r}_1, j = 2, 3$. Hence the unknowns that remain in the solution of the forward kinematics are $\mathbf{q}_x$, $\mathbf{q}_y$ and the position vector $\mathbf{p}$. Accordingly, nine constraint equations can be written as

$$(\mathbf{p} + \mathbf{Q}\mathbf{d}_i - \mathbf{r}_i)^T(\mathbf{p} + \mathbf{Q}\mathbf{d}_i - \mathbf{r}_i) - l_{i4}^2 = 0, \quad i = 1, 2, 3 \tag{18}$$

$$(\mathbf{r}_1 - \mathbf{p})^T \mathbf{q}_z = 0 \tag{19}$$

$$\mathbf{Q}^T\mathbf{Q} - \mathbf{1} = 0 \tag{20}$$

where $\mathbf{1}$ stands for the 3×3 identity matrix. Also, it should be noted that (20) provides only five constraint equations since $\mathbf{q}_z$ is readily computed from (17). Combining these nine constraint equations yields a system of 9 nonlinear equations that can be written as

$$\mathbf{f}(\mathbf{x}) = \mathbf{0} \tag{21}$$

in which $\mathbf{x} = [\mathbf{q}_x^T \ \mathbf{q}_y^T \ \mathbf{p}^T]^T$. The Newton-Raphson method is then used to solve this system of equations. At iteration k, the computations can be written as

$$\text{Solve} \quad \mathbf{F}(\mathbf{x}^{(k)})\boldsymbol{\delta}^{(k)} = -\mathbf{f}(\mathbf{x}^{(k)}) \quad \text{for} \quad \boldsymbol{\delta}^{(k)} \tag{22}$$

$$\mathbf{x}^{(k+1)} = \mathbf{x}^{(k)} + \boldsymbol{\delta}^{(k)}, \quad k = 0, 1, \cdots \tag{23}$$

where matrix $\mathbf{F}(\mathbf{x})$ is the partial derivative of $\mathbf{f}(\mathbf{x})$ with respect to $\mathbf{x}$ and is of dimension 9×9. The procedure is stopped when the equations are satisfied within a predetermined accuracy. With a proper initial guess (which is usually available in the tracking of a trajectory), the procedure converges very quickly (typically less than 4 iterations are required).

B. Inverse Kinematics

The solution of the inverse kinematics of kinematically redundant serial or parallel robots typically requires the use of numerical iterative methods based on the velocity equations (see for instance [6]). However, in the proposed KRHR, the arrangement of the redundant links and the moving platform readily leads to a simple analytical solution of the inverse kinematics. Indeed, referring to Fig. 2, angles $\beta_i, i = 1, 2, 3$ are determined by the opening of the gripper for two of the legs and by the avoidance of type II singularities for the third leg. In fact, for the third leg, angle β_i is maintained at a constant value that is guaranteed to avoid singularities and mechanical limits for any value of the other two β_i angles. Then, vectors $\mathbf{r}_i, i = 1, 2, 3$ can be simply written in terms of the position and orientation of the moving platform and angles β_i. At last, the analytical inverse kinematic solution of the proposed KRHR is solved by solving the inverse kinematic problem of each (RR-RRR) leg analytically. It should be noted that the analytical solution is computationally efficient, consistent and conservative[1], which is a desirable property for a redundant robot.

IV. Prototyping

A prototype of the proposed KRHR was designed and built. A CAD model of the prototype is shown in Fig. 3 and a photograph of the prototype is shown in Fig. 4. In the prototype, two of the redundant degrees of freedom are used to operate the jaws of a gripper, as illustrated in Fig. 5. The third redundant degree of freedom is used to maintain angle β_3 at a value that guarantees that the robot is far from type II singular configurations. Because singularities can always be avoided, the robot has a large workspace, especially in orientation. Rotations of $\pm90^\circ$ can be performed around each of the Cartesian axes in a significant portion of the positioning workspace.

The actuators used are EC 90 flat, brushless, 260 W, from Maxon. They are equipped with encoders that provide a resolution of 16384 counts per turn using quadrature. In order to ensure backdrivability, no mechanical transmissions are used, i.e., a direct drive arrangement is chosen. The total mass of the robot (including the 9 actuators) is approximately 11.2 kg including 8.8 kg for the motors and 2.8 kg for the counterweights, i.e., most of the mass is located very close to the base. Therefore, the inertia of the moving parts is low due to the lightweight construction of the legs and gripper and due to the fact that the gripper is operated from the motors located at the base (no actuator needs to be mounted on the end-effector to operate the gripper).

V. Control for pHRI

Collaborative robots include a control mode in which the robot can be guided manually by direct physical contact between the user and the robot. In the vast majority of collaborative robots, this mode of operation is based on admittance

[1]By conservative, we mean that a given set of inputs (pose of the platform and angles $\beta_i, i = 1, 2, 3$) always produces the same joint coordinates regardless of the trajectory followed by the robot.

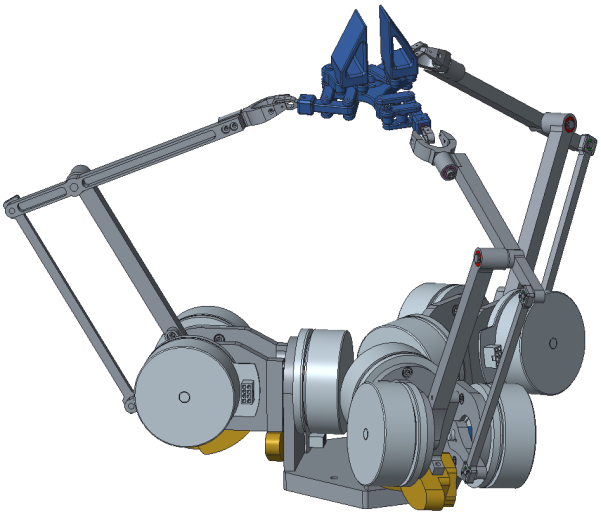

Fig. 3. CAD model of the proposed hybrid robot.

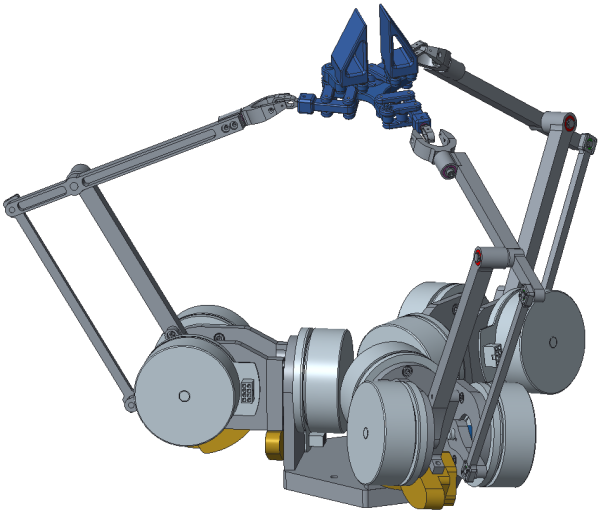

Fig. 4. Photograph of the prototype of the proposed hybrid robot.

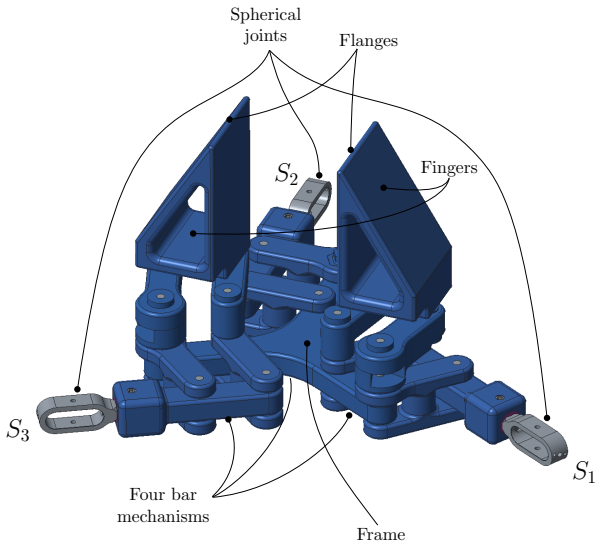

Fig. 5. CAD model of the mechanism driving the gripper implemented in the prototype.

control using either a force/torque sensor mounted at the end-effector of the robot or joint torque sensors. Indeed, impedance control cannot be used because such robots are not backdrivable, due to the gear transmissions mounted between the actuators and the robot joints. Although admittance control based on force/torque sensors is a functional approach, it greatly limits the bandwidth of the interaction between the human user and the robot and therefore makes the interaction less intuitive.

The robot proposed in this paper uses direct-drive transmissions, which makes it completely back-drivable. Moreover, because of the hybrid architecture of the robot, the actuators are located close to the base and hence the inertia of the moving parts is small. Therefore, impedance control can be used, thereby greatly increasing the bandwidth of the human/robot interaction.

In an impedance control scheme, the robot is moved by the user. This motion is then perceived by the joint encoders and the actuators react with an appropriate torque, according to the desired dynamics [7]. This control scheme is well understood for conventional robots. However, the proposed robot is kinematically redundant, which makes the direct application of an impedance controller less straightforward. Indeed, infinitely many actuated joint configurations correspond to a given Cartesian pose of the platform. Hence, if the user is free to move the end-effector of the robot, a strategy must be developed to ensure the proper joint motions of the robot. The control strategy used in this robot is as follows. First, the motion imparted to the robot end-effector by the user is detected by the actuated joint encoders. Using the encoder values, the direct kinematics of the robot are solved to determine the pose of the platform and the opening of the gripper. Given the pose of the platform and the gripper opening, the inverse kinematic problem is then solved to determine the proper configuration of the robot, i.e., the actuated joint configuration that matches the pose of the platform and that drives the third redundant degree of freedom to a prescribed configuration that is far away from singularities. Using this approach, the robot follows the input of the user while always keeping a configuration that is free from singularities and far from mechanical limits.

The desired behaviour of the robot is that the user can move the end-effector as smoothly as possible and that the end-effector remains in its current pose when the user lets go of it. This functionality is implemented using the following approach, as illustrated in the block diagram of the controller given in Fig. 6. In order to allow users to guide the robot freely, the position controller at each joint includes a function called ‘reference update’ as shown in Fig. 6. A double threshold strategy is used in this function. A velocity threshold is first defined in order to determine whether the user desires to move or stop the guidance. The reference position is then updated continuously as long as the velocity remains higher than this threshold. The second threshold is a position threshold. It is activated whenever the robot comes to rest. The robot then reverts back to position control and this threshold deals with the static error and

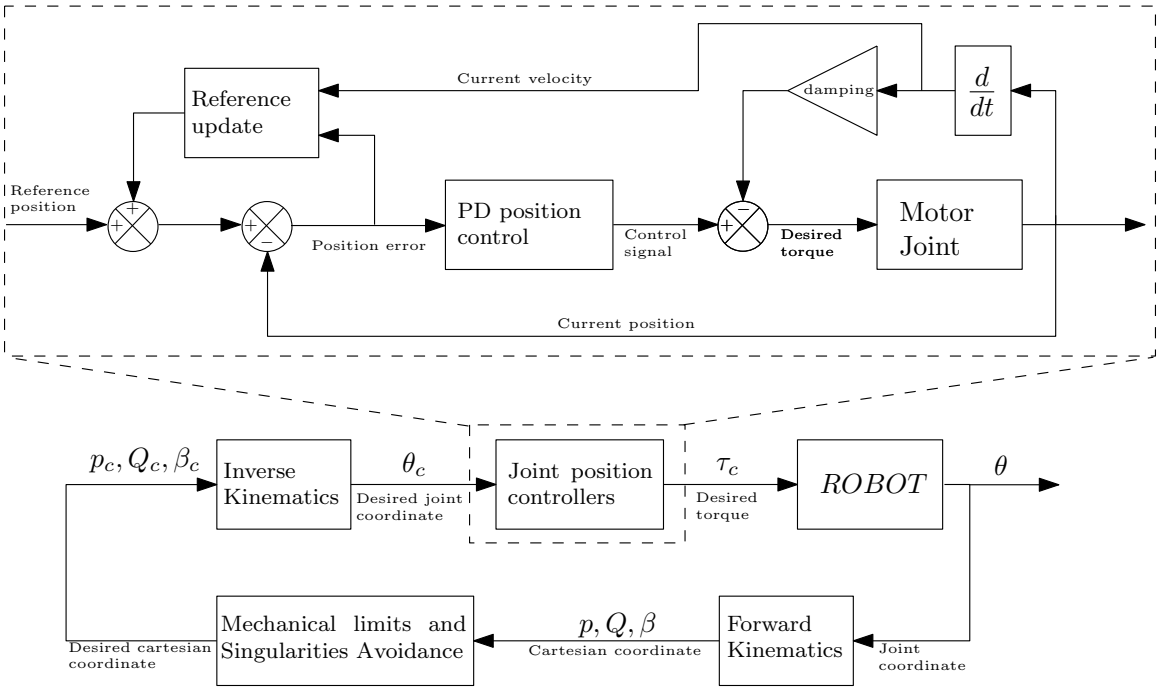

Fig. 6. Block diagram of the controller for the interactive mode.

inertial movement. A small damping is also added so that the motion is more natural for the user. This strategy enables the user not to feel any resistance, except for a small effort to overcome the damping, while ensuring the stability of the robot in the motionless state.

VI. Conclusion

This paper proposes a novel kinematically redundant hybrid robot for intuitive physical human-robot interaction. The robot is constructed using a (quasi-parallel) hybrid kinematic architecture, which allows one to use direct-drive actuators, thereby making the robot backdrivable. Backdrivability then opens the possibility of using an impedance control scheme (instead of admittance) which drastically increases the bandwidth of the interaction. The control scheme is based on the successive computation of the direct kinematics and the inverse kinematics of the robot, which produces the desired interaction dynamics while maintaining the robot in a desirable singularity-free configuration. Low-impedance highly reactive collaborative robots can find applications in a variety of areas and therefore the proposed robot is a promising concept for physical human-robot interaction.

References

[1] V. Duchaine and C. M. Gosselin, "Investigation of human-robot interaction stability using Lyapunov theory," in *IEEE International Conference on Robotics and Automation*, 2008, pp. 2189–2194.

[2] V. Duchaine, B. M. St-Onge, D. Gao, and C. Gosselin, "Stable and intuitive control of an intelligent assist device," *IEEE Transactions on Haptics*, vol. 5, no. 2, pp. 148–159, 2012.

[3] N. Badeau, C. Gosselin, S. Foucault, T. Laliberté, and M. E. Abdallah, "Intuitive physical human–robot interaction: Using a passive parallel mechanism," *IEEE Robotics and Automation Magazine*, vol. 25, no. 2, pp. 28–38, 2018.

[4] C. Gosselin and J. Angeles, "Singularity analysis of closed-loop kinematic chains," *IEEE Transactions on Robotics and Automation*, vol. 6, no. 3, pp. 281–290, 1990.

[5] K. Wen, D. Harton, T. Laliberté, and C. Gosselin, "Kinematically redundant (6+3)-dof hybrid parallel robot with large orientational workspace and remotely operated gripper," in *IEEE International Conference on Robotics and Automation*, 2019.

[6] C. Gosselin and L.-T. Schreiber, "Kinematically redundant spatial parallel mechanisms for singularity avoidance and large orientational workspace," *IEEE Transactions on Robotics*, vol. 32, no. 2, pp. 286–300, 2016.

[7] R. J. Anderson and M. W. Spong, "Hybrid impedance control of robotic manipulators," *IEEE Journal on Robotics and Automation*, vol. 4, no. 5, pp. 549–556, 1988.